Cerebral Cortex, May 2017;27:3015–3027

doi:10.1093/cercor/bhw096
Advance Access Publication Date: 26 May 2016

ORIGINAL ARTICLE

Opposing Effects of Maternal Hypo- and Hyperthyroidism on the Stability of Thalamocortical Synapses in the Visual Cortex of Adult Offspring

Marie-Therese J. Strobl[1,2], Daniel Freeman[1], Jenica Patel[1], Ryan Poulsen[1], Christopher C. Wendler[1], Scott A. Rivkees[1] and Jason E. Coleman[1]

[1]Department of Pediatrics, Child Health Research Institute, University of Florida College of Medicine, Gainesville, FL 32610, USA and [2]Department of Nuclear Medicine, University Medical Center, University RWTH Aachen, 52074 Aachen, Germany

Address correspondence to Jason E. Coleman, Department of Pediatrics, UF COM, ARB R1-102, 1200 Newell Drive, Gainesville, FL 32610, USA. Email: jcoleman@ufl.edu

Abstract

Insufficient or excessive thyroid hormone (TH) levels during fetal development can cause long-term neurological and cognitive problems. Studies in animal models of perinatal hypo- and hyperthyroidism suggest that these problems may be a consequence of the formation of maladaptive circuitry in the cerebral cortex, which can persist into adulthood. Here we used mouse models of maternal hypo- and hyperthyroidism to investigate the long-term effects of altering thyroxine (T4) levels during pregnancy (corresponding to embryonic days 6.5–18.5) on thalamocortical (TC) axon dynamics in adult offspring. Because perinatal hypothyroidism has been linked to visual processing deficits in humans, we performed chronic two-photon imaging of TC axons and boutons in primary visual cortex (V1). We found that a decrease or increase in maternal serum T4 levels was associated with atypical steady-state dynamics of TC axons and boutons in V1 of adult offspring. Hypothyroid offspring exhibited axonal branch and bouton dynamics indicative of an abnormal increase in TC connectivity, whereas changes in hyperthyroid offspring were indicative of an abnormal decrease in TC connectivity. Collectively, our data suggest that alterations to prenatal T4 levels can cause long-term synaptic instability in TC circuits, which could impair early stages of visual processing.

Key words: development, synapse, thalamocortical, thyroid hormones, two-photon

Introduction

Thyroid hormones (TH) play a critical role in fetal development including neurogenesis and the formation of neural circuitry important for sensory processing (Ruiz-Marcos et al. 1979, 1983; Koibuchi and Chin 2000; Berbel et al. 2010; Horn and Heuer 2010; Gilbert and Lasley 2013; Rovet 2014). Thyroxine (T4) serves as the precursor for the active form of TH, triiodothyronine (T3), and is maternally supplied during pregnancy (Calvo et al. 1990, 2002; Rovet 2014). Consequently, children born from mothers who are hypothyroid during pregnancy are at high risk for long-term neurological and cognitive deficits, including impairments in core visual functions and visual processing (Mirabella et al. 2005; Rovet and Simic 2008; Simic et al. 2013; Rovet 2014). Indeed, it is appreciated that even relatively small reductions in maternal T4 levels are associated with poor neurodevelopmental outcome (Zoeller and Rovet 2004; Horn and Heuer 2010). Infants born premature with mild, transient hypothyroidism are also at risk (Delahunty et al. 2010; Williams et al. 2012). In addition, while there are reports that excessive T4 levels during pregnancy or over-treatment of hypothyroidism are also associated with neurodevelopmental abnormalities (Daneman and Howard 1980; Kopelman 1983; Bongers-Schokking and de Muinck Keizer-Schrama 2005),

the effects of prenatal hyperthyroidism are not as well understood.

In animal models, several studies have shown that perinatal hypothyroidism can cause meso- and microscale disturbances in the maturation of neuronal connectivity in sensory cortices (Berbel et al. 1985, 1993, 2010; Ipina et al. 1987; Gravel and Hawkes 1990; Gravel et al. 1990; Ruiz-Marcos et al. 1994; Navarro et al. 2014). The development and maturation of callosal and thalamocortical (TC) axonal projections are particularly vulnerable to severe TH insufficiency. Severe hypothyroidism during pre- and postnatal development causes reductions in TC axon innervation density, branching, and bouton density in individual barrels of rat somatosensory cortex (Auso et al. 2001). Rats exposed to a combination of pre- and postnatal hypothyroidism exhibit abnormal laminar connectivity of callosal axons in auditory and visual cortices in adulthood (Berbel et al. 1985, 1993; Gravel and Hawkes 1990; Gravel et al. 1990; Lucio et al. 1997). It is likely that such defects in axonal connectivity, together with reductions in inhibitory interneurons caused by late gestational hypothyroidism, can render cortical circuits prone to abnormal plasticity and maladaptation throughout life (Berbel et al. 1996; Gilbert et al. 2007, 2014). Finally, there is some evidence from work in rat cerebellar cortex and hippocampus that long-term postnatal hyperthyroidism also has a clear effect on the maturation of neural circuitry at the structural level (Nicholson and Altman 1972; Lauder 1977, 1978). However, there is a paucity of animal studies demonstrating the effects of early hyperthyroidism on neocortical circuit development and long-term function (Marta et al. 1998; Bruno et al. 2003; Ahmed et al. 2012).

Recent work using chronic two-photon imaging of axons in live mice has shown that axons exhibit ongoing changes in connectivity in sensory cortices throughout adulthood (De Paola et al. 2006; Gogolla et al. 2007). Branches of cortico-cortical and TC axons, as well as individual synapses, can be monitored over time using this approach. Prior work has shown that large-scale synaptic remodeling of TC axons occurs in layer 1 of adult somatosensory cortex (De Paola et al. 2006). This remodeling largely occurs through the extension (growth) and retraction (loss) of distal axonal branch tips, which is accompanied by the gain and loss of en passant boutons (EPBs). Importantly, such structural changes are well correlated with functional plasticity (Oberlaender et al. 2012; Canty et al. 2013; Grillo et al. 2013). Anatomical changes to TC axons and synapses in primary visual cortex (V1) accompany functional changes in neuronal activity that underlie synaptic plasticity (Antonini and Stryker 1993; Wiesel 1999; Coleman et al. 2010; Khibnik et al. 2010). Thus, monitoring structural changes to TC axons and EPBs can provide an anatomical readout for steady-state changes in connectivity that could influence cortical function.

The aim of this study was to improve our understanding of the long-term effects of prenatal hypo- and hyperthyroidism on the ongoing maintenance of neuronal structure and function in the cerebral cortex and ultimately, how these conditions affect visual learning and behavior. While rat models for studying pre- and/or postnatal hypothyroidism are widely used, mouse models are not as common. Furthermore, rat and mouse models of prenatal hyperthyroidism are even less common and the effects of excessive T4 on neural development and long-term neural function are poorly understood. Therefore, here we developed mouse models of maternal hypo- and hyperthyroidism by administering methimazole (MMI) or levo-thyroxine (LT4) during pregnancy to lower or raise maternal T4 levels, respectively. We then performed chronic two-photon imaging of TC axons and EPBs in V1 of adult offspring. We found that both prenatal hypo- and hyperthyroidism are associated with atypical steady-state dynamics of TC axons and associated synapses in V1 of adult mice.

Materials and Methods

Animals

Male and female C57BL/6 mice (6–8 weeks) were obtained from Charles River and housed under 12-h light/dark conditions at the University of Florida (UF). All animal procedures were performed in accordance with NIH *Guide for the Care and Use of Laboratory Animals* (NIH publication no. 86-23, revised 1987) and were approved by the Institutional Animal Care and Use Committee at UF. As described below, measures were taken to minimize pain or discomfort. Harem matings were used for producing timed pregnancies. Pups were weaned at postnatal day (P) 18 following surgeries as described below. A total of 86 pregnant dams were used for this study (49 of which gave birth to surviving pups, Supplementary Table 1). A detailed breakdown of how these animals and their offspring were used throughout the study is provided in Supplementary Tables 2 and 3.

Maternal Hypo- and Hyperthyroid Mouse Model and Thyroxine (T4) Assays

Pregnant dams were randomly assigned to 1 of 3 experimental groups. Dams were treated daily between embryonic age (E) 6.5 and E18.5 with vehicle ($n = 5$), MMI (20 mg/kg in water, $n = 6$), or LT4 (0.2 mg/kg in PBS, $n = 8$) (Sigma-Aldrich, St. Louis, MO). MMI was delivered intragastrically with an oral gavage needle and LT4 was delivered via intraperitoneal injection (Fig. 1A). Control mice received corresponding doses of vehicle. Pups remained with their mothers until weaning. In a separate group of mice, 100 μL of blood was collected from the dams on days corresponding to E13.5 and E18.5 via the facial vein (Supplementary Table 2; control, $n = 10$; MMI, $n = 7$; LT4, $n = 5$–7). Once the pups reached P5, the mother and her pups were euthanized with CO_2 and blood was then immediately collected from the mother by cardiac puncture (control, $n = 9$; MMI, $n = 7$; LT4, $n = 5$) and from pups (control, $n = 6$; MMI, $n = 5$; LT4, $n = 3$) after decapitation. Blood samples were centrifuged at 3000 rpm for 10 min. Sera were decanted and frozen at −80°C until use. T4 levels were determined using a mouse/rat T4 ELISA according to the manufacturer's instructions (GenWay Biotech, Inc., San Diego, CA).

Lentiviral Vector

Lentiviral vector (LV-Syn-farGFP; stock# VSVG.HIV.SIN.ratSyn.FarGFP.WP; ~1×10^9 transducing units/mL) suspended in PBS was prepared by the University of Pennsylvania Vector Core. The transducing plasmid vector carrying the expression cassette pLL3.7-Syn-farGFP was a gift from Yasunobu Murata and Martha Constantine-Paton. The expression cassette consisted of a 1.2 kb fragment of the rat synapsin promoter (Dittgen et al. 2004) driving farnesylated GFP. The synapsin promoter fragment (from pFSy (1.1)GW, a gift from Pavel Osten, Addgene plasmid # 27232) was inserted between the Not1 and Age1 sites of pLL3.7 (a gift from Luk Parijs, Addgene plasmid # 11795) to create pLL3.7-Syn-GFP. The farnesylated GFP was constructed by inserting annealed oligonucleotides (sense = 5′-GTACAAGTCCGGACTCAGATCTAAG CTGAACCCTCCTGATGAGAGTGGCCCCGGCTGCATGAGCTGCAA GTGTGTGCTCTCCTGAG-3′; antisense = 5′-AATTCTCAGGAGAGC ACACACTTGCAGCTCATGCAGCCGGGGCCACTCTCATCAGGAGGG TTCAGCTTAGATCTGAGTCCGGACTT-3′) between the BsrGI and

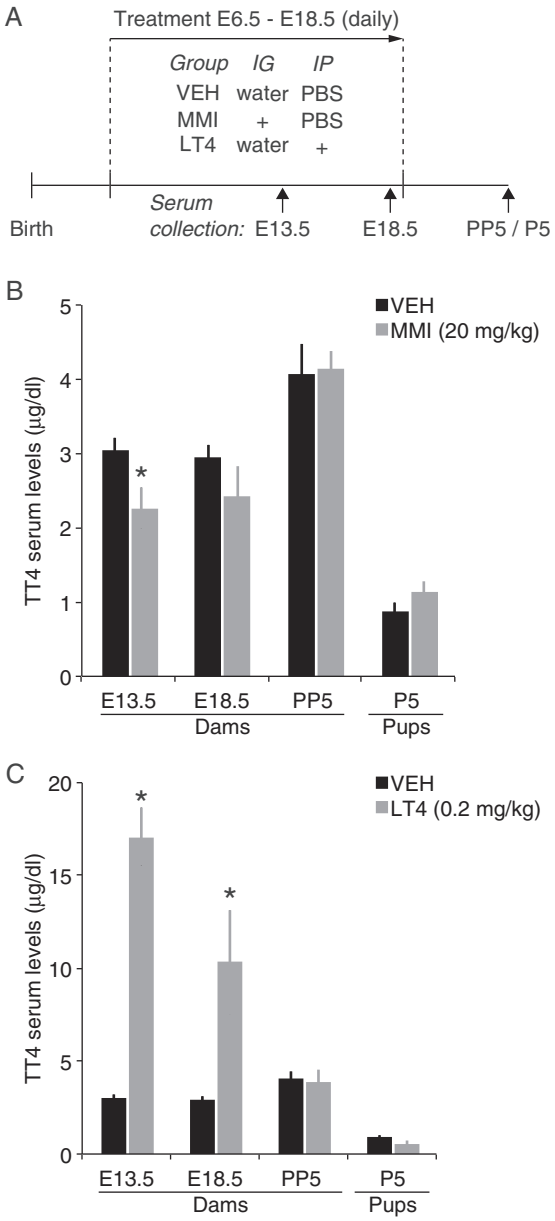

Figure 1. Summary of the effects of MMI and LT4 administration on serum T4 levels. (*A*) Experimental design. (*B*) Total T4 (TT4) levels in vehicle control (VEH) and MMI-treated mice, and (*C*) in VEH and LT4-treated mice. The same vehicle data are shown in (*B*) and (*C*) (means ± SEM *$P < 0.05$ vs. VEH; IG, intragastric; IP, intraperitoneal).

EcoRI sites of the 3′-end of GFP in pLL3.7-Syn-GFP to create pLL3.7-Syn-farGFP.

Cranial Window Surgery

Mice (P18) were anesthetized with a mixture of ketamine and xylazine and 0.1–0.5% isoflurane and prepared for cranial window surgeries as described (Mostany and Portera-Cailliau 2008), along with the following modifications. Because prior work has already shown that TC axons exhibit steady-state structural dynamics in sensory cortices of adult male mice (De Paola et al. 2006), only male mice were used for the two-photon imaging study. Prior to the craniotomy, a small headpost was affixed to the skull with glue and bone cement anterior to bregma and used to secure the head to a modified stereotaxic frame. After adjusting the animal's head to lie in the stereotaxic plane, an injection pipet was placed 1.70 mm posterior from bregma and 3.30 mm lateral from the midline suture, the point was marked on the skull, and then moved out of the way. The head was rotated 30° clockwise, and lateral movements were made to reposition the pipet over the marked site and again raised out of the way. Immediately following the craniotomy, care was taken to minimize brain compression and gently penetrate the dural surface with the injection pipet. The pipet was lowered 2.60 mm below the ventral surface to target the dorsal lateral geniculate nucleus (dLGN), the visual portion of the thalamus that contains relay neurons that project axons directly to V1. A Nanoliter 2010 injector driven by a Micro 4 pump controller (World Precision Instruments) was used to slowly infuse 130 nL of LV-Syn-farGFP at 15 nL/s at 2.60, 2.45, and 2.30 mm dorsoventrally. The pipet was left in place for 5–10 min after the last injection and then slowly removed. A 4.0-mm glass coverslip (No. 1 thickness, World Precision Instruments) was placed over the dura and anchored to dry skull using high-viscosity cyanoacrylate glue. Glue was applied all around the coverslip to create an airtight seal. Bone cement (Palacos-R) was then applied over the glue and to the skull immediately surrounding the window. Any remaining exposed skull was covered with dental cement (Orthojet) and the animals were allowed to recover with heat after receiving lactated Ringer's solution (0.1–0.2 cc). Animals were given carprofen (50 mg/kg) for management of postoperative pain and discomfort and singly housed until imaging.

Two-photon Imaging

Five male mice were prepared for imaging from each group, but some were subsequently excluded from the study because their cranial windows were not optically clear and could not be imaged (Supplementary Table 3). Imaging of TC axons in V1 was performed using a customized Thorlabs B-scope two-photon laser scanning microscope fitted with a Ti::Sapphire light source (Vision II, Coherent). GFP-labeled axons were imaged at a wavelength of 930 nm. Three-dimensional images (image Z-stacks) were comprised of a "stack" of two-dimensional XY images where each image in the stack represented a single step of 1.0 µm in the focal plane (i.e., Z-dimension). One to 3 image Z-stacks were acquired on each imaging day using a Nikon 25× water-immersion lens (N.A. 1.1). Laser power was incrementally increased by the acquisition software (Thorimage) with increasing cortical depth and ranged from 20 to 60 mW at the objective. Two imaging sessions (day 1 and day 2; 2048 × 2048 pixels; pixel scale = 0.5 × 0.5 µm) were performed for each animal (mean imaging interval = 44.2 ± 6.8 days; day 1 mean age = 62.4 ± 2.5 days, range = 55–83 days; day 2 mean age = 106.6 ± 7.5 days, range = 82–127 days). Subjects were anesthetized using 3.0% isoflurane and maintained on 1.0–1.5% isoflurane during imaging sessions. Imaging sessions typically lasted 1–2 h depending upon the number of regions imaged. Axonal branches were imaged up to ~300 µm dorsoventrally from the pia, which corresponds to layer 1 and layer 2/3, but images typically spanned between 20 and 150 µm from the pial surface. In all but 2 cases, the imager was blind to treatment history.

Histology

A separate group of animals in another study was used to verify the accuracy of targeting injections to the dLGN and two-photon

imaging in V1. For cortical labeling of the imaged area, a small hole was drilled in the glass coverslip using a diamond bit (1/12″ bit, 3/32″ shank; DiamondBurs.Net, LLC) fitted to a high-speed micro drill (Fine Science Tools). Mice were perfused and their tissue was processed as previously described (Coleman et al. 2009, 2010). One hundred micrometer-thick serial sections were cut on a vibratome. In some cases, the location of lentivirus injections, axon labeling and imaging in V1 was confirmed post hoc by marking the imaged region with a retrograde tracing dye (cholera toxin B-subunit tagged with Alexa-647 fluorescent dye, Invitrogen) (Coleman et al. 2009).

Image Analysis

Only imaged regions and structures that could be clearly identified in both images were used for analysis. All analyses were performed blind to condition using the "simple neurite tracer" plug-in for FIJI/ImageJ image processing software (http://fiji.sc/wiki/) and custom-written software for MATLAB (MathWorks). In some cases, a second independent, blind researcher confirmed branch tip identification and measurement analysis. The change in length (ΔL) of identified axonal branch tips between images was calculated as follows: $\Delta L = L_{day(2)} - L_{day(1)}$. To estimate measurement noise (De Paola et al. 2006), the distance between 5 and 10 fiduciary points in each image Z-stack was measured and the average used to compute a measurement noise factor, σ, for each stack. σ_{noise} was defined as the average of σ (1.38 μm). Therefore, branch tip length changes greater than σ_{noise} are greater than the stochastic fluctuations in the images due to changes in head position, breathing, and blood flow. Each branch tip was considered an n within each group (control, $n = 261$ from 3 mice; MMI, $n = 116$ from 4 mice; LT4, $n = 220$ from 3 mice). For comparisons of the magnitude of branch tip extensions and retractions, positive- and negative-going values were separated and means for each group were calculated using only values that were $>2\sigma_{noise}$, a threshold that reliably represented significant branch tip movement.

Prior work has shown that synapses can be readily identified and objectively quantified via two-photon imaging of GFP-labeled TC axons and careful analysis of EPBs (De Paola et al. 2006; Grillo et al. 2013). Therefore, EPBs along partial axons reconstructed from spared branches that were clearly visible in imaged regions were scored and classified as follows. First, segmentation of each image Z-stack was performed using the "fill out" function of the simple neurite tracer plug-in and a threshold of 0.5–0.8, which generated a segmented 3D image of only traced branches. Putative EPB regions, defined as bright swellings along the axon backbone, were identified using local intensity maxima in thresholded maximum-intensity Z-projections of the segmented axon arbor tracings from day 1 images. The Cartesian coordinates of putative EPBs were stored using the region of interest (ROI) manager tool in Fiji/ImageJ. ROIs (7 × 7 pixels, 3.5 × 3.5 μm) were then manually adjusted for the day 1 images and placed over corresponding EPB locations in the day 2 images. The brightness of each bouton ROI was then calculated by summing the gray values within each ROI in segmented image Z-stacks. Next, 10-pixel (5-μm) wide ROIs were placed along the axonal backbone within 6 μm of each bouton ROI. If the bouton ROIs were too tightly packed, measurements were placed at the ends of each cluster or the closest axonal backbone region. The brightness of each axonal backbone ROI was then calculated by summing the gray values in segmented image Z-stacks.

Putative EPBs were then classified as stable, lost, or gained based on a threshold that was derived as follows. The fold-brightness of each EPB was calculated by dividing it by the average of the 2 nearest axonal backbone brightness values (EPB_{fold}). The standard deviation of EPB_{fold} for all boutons within a given image (std_{fold}) was then used to classify each individual ROI (i.e., putative bouton) as follows:

$$\text{Stable EPB} = \text{day 1}(EPB_{fold} > 0.5 \times std_{fold}) \text{ and. . .}\\ \text{day 2}(EPB_{fold} > 0.5 \times std_{fold})$$

$$\text{EPB loss} = \text{day 1}(EPB_{fold} > 0.5 \times std_{fold}) \text{ and. . .}\\ \text{day 2}(EPB_{fold} < 0.5 \times std_{fold})$$

$$\text{EPB gain} = \text{day 1}(EPB_{fold} < 0.5 \times std_{fold}) \text{ and. . .}\\ \text{day 2}(EPB_{fold} > 0.5 \times std_{fold})$$

Similar measurements and criteria have been shown to reliably predict the presence of synapses in TC axons in mouse neocortex (De Paola et al. 2006; Grillo et al. 2013). The percentage of dynamic, lost, and gained EPBs per axon was calculated as follows: % dynamic = 100 × (#lost + #gained)/(total); % loss = 100 (#lost/total); % gain = 100(#gained/total). In this study, a total of 2678 putative EPBs were analyzed and each animal was considered an n within each group. The average number of putative EPBs that were scored for day 1 (i.e., day 1($EPB_{fold} > 0.5 \times std_{fold}$)) for each animal was not significantly different across groups (control: 174.3 ± 66.8, MMI: 145.7 ± 28.2, LT4: 167.3 ± 91.2; $P = 0.84$, Kruskal–Wallis (K–W) test).

Statistics

The unpaired t-test was used to test for differences in sera T4 levels between control and MMI or LT4 groups. One-way ANOVA on ranks (K–W test) was used to test for differences in branch tip length changes and EPB dynamics among the 3 groups. Group comparisons were determined a priori. A nonparametric bootstrap test (10 000 resampling iterations) was used to estimate the 95% confidence interval (CI) for the mean differences between groups in order to test the null hypothesis that the difference was 0. Bootstrap test P-values were calculated from the 95% CI as described (Altman and Bland 2011). Differences between group distributions of axonal length changes were determined using the two-sample Kolmogorov–Smirnov test. Significance was set at $P < 0.05$, and all tests were performed using MATLAB.

Results

Mouse Models for Maternal Hypo- and Hyperthyroidism

While rat models for studying pre- and/or postnatal hypothyroidism are widely used, mouse models are not as common. Furthermore, rat and mouse models of prenatal hyperthyroidism are even less common and the effects of excessive T4 on neural development and long-term neural function are poorly understood. Therefore, we first sought to establish mouse models of prenatal hypo- and hyperthyroidism. MMI, which interferes with T3 and T4 synthesis by blocking the thyroperoxidase enzyme in the thyroid gland (Cooper et al. 1984), has been widely used to induce hypothyroidism in both pre- and postnatal rats and is nonteratogenic in mice (Gilbert and Lasley 2013; Mallela et al. 2014).

We first tested if daily MMI or LT4 administration could induce hypothyroidism or hyperthyroidism, respectively, in pregnant mice (Fig. 1A and Supplementary Tables 1 and 2). Overall, daily doses of MMI (20 mg/kg), LT4 (0.2 mg/kg), or vehicle administered from E6.5 to E18.5 did not cause any qualitatively noticeable

changes in behavior in treated mice or their offspring. For control dams, 90% (26/29) gave birth after E18.5. The birth rate was similar for MMI-treated dams as 100% gave birth after E18.5 (22/22). In contrast, the birth rate was lower for LT4-treated dams, 69% (24/35) of which gave birth after E18.5 (31% gave birth 1–2 days earlier). However, the survival rate of the litters from pregnant dams in all groups that gave birth after E18.5 was similar across groups (control: 65% (17/26), MMI: 73% (16/22), LT4: 67% (16/24)). To test the effects of each drug on circulating total T4 (TT4) levels, we measured TT4 approximately midway through the treatment period (E13.5), at the end of treatment (E18.5), and 5 days postpartum (Fig. 1A). MMI treatment caused a significant decrease in TT4 at E13.5 (Fig. 1B; MMI: 2.27 ± 0.27 µg/dL, $n = 7$; control: 3.05 ± 0.16 µg/dL, $n = 10$; $P = 0.018$, unpaired t-test), but was not significantly different at E18.5 (MMI: 2.43 ± 0.41 µg/dL, $n = 7$; control: 2.94 ± 0.19 µg/dL, $n = 10$; $P = 0.221$, unpaired t-test). LT4-treatment caused a significant increase in TT4 at E13.5 (Fig. 1B; 17.01 ± 1.55 µg/dL, $n = 7$; $P < 0.0001$, unpaired t-test vs. control) and E18.5 (10.34 ± 2.80 µg/dL, $n = 5$; $P = 0.0020$, unpaired t-test vs. control). The 26% decrease in TT4 at E13.5 in the MMI group was similar to decreases observed in pregnant rats at ~E10 with a "low dose" of MMI (0.02% w/v; 1 ppm) or propylthiouracil (1 ppm) delivered via drinking water (Ahmed et al. 2010; Lasley and Gilbert 2011). These values are consistent with mild maternal hypothyroidism. By day 5 postpartum, TT4 reached normal levels in both MMI and LT4 groups (control: 4.01 ± 0.40 µg/dL, $n = 9$; MMI: 4.13 ± 0.26 µg/dL, $n = 7$; LTF: 3.91 ± 0.63 µg/dL, $n = 5$; $P = 0.918$, unpaired t-test, control vs. MMI; $P = 0.817$, unpaired t-test, control vs. LT4).

To determine whether T4 levels were affected in neonate offspring, TT4 levels were measured in P5 pups from control, MMI, and LT4 groups. TT4 levels in MMI and LT4 pups were not significantly different from control pups (Fig. 1B; control: 0.88 ± 0.10 µg/dL, $n = 6$; MMI: 1.15 ± 0.14 µg/dL, $n = 5$; LT4: 0.51 ± 0.21 µg/dL, $n = 3$; $P = 0.144$, unpaired t-test, control vs. MMI; $P = 0.105$, unpaired t-test, control vs. LT4). Together, these data show that MMI and LT4 administration during pregnancy cause transient hypo- and hyperthyroidism, respectively, during fetal development without affecting postnatal TT4 levels.

Opposing Effects of Prenatal Hypo- and Hyperthyroidism on the Stability of TC Axonal Branches

Previous studies have demonstrated that TH insufficiency during pre- and postnatal development can incur long-term consequences on the cellular composition (Plioplys et al. 1986; Gravel and Hawkes 1990) and anatomical structure of cortical axons (Gravel and Hawkes 1990; Gravel et al. 1990; Berbel et al. 1993; Lucio et al. 1997; Auso et al. 2001). However, there is little or no information regarding the effects of maternal hypo- and hyperthyroidism on the ongoing structural stability of cortical axons. Therefore, we next sought to characterize the effect of prenatal TH levels on the steady-state dynamics of TC circuitry in V1 of adult mice by measuring changes in TC axonal branch tips. To do this, we first selectively labeled TC axons in V1 with a membrane-tagged GFP that enhances axonal labeling by targeted injection of LV-Syn-farGFP into the dLGN (Fig. 2A–C). Following 3–5 weeks of recovery, we began longitudinal imaging of TC axons (Fig. 2D,E). In addition to post hoc histological confirmation, we were confident that imaged axons were indeed of TC origin due to the fact that they exhibited laminar-specific patterning of horizontal branches characteristic of TC axons, which were dense in layer 1 (down to ~150–200 µm) and were reduced as the focal plane progressed ventrally until reaching deeper into layer 2/3 (~300 µm) and layer 4 (~400–450 µm) where the density of horizontally projecting branches was again increased, as can be seen in the representative image shown in Figure 2C. Furthermore, the absence of cell bodies in imaged areas provided further confirmation that injections were indeed restricted to the dLGN/thalamus, and that the axons in V1 were not of cortical origin.

To determine whether the density of labeled TC axons innervating layer 1 differed among groups, we estimated the density of labeled TC axons in the imaged volumes. While there was a noticeable increase in the variability of labeled TC axon density in the MMI group, there were no significant differences detected across all groups (Supplementary Fig. 1).

To examine the steady-state dynamics of TC axon structure in V1, we quantified branch tip dynamics by measuring changes in the length of distal axon tips in 2 images separated by a 1–2 month interval (Fig. 3A). Consistent with previous reports of steady-state TC axon dynamics monitored by two-photon imaging in somatosensory cortex, control TC axons exhibited both extensions and retractions of their branch tips, examples of which are shown in Figure 3A (De Paola et al. 2006). Overall, there were significant differences in the net change of axonal branch tips between control and treatment groups ($P = 0.026$, K–W test; control, $n = 261$ branch tips from 3 mice; MMI, $n = 116$ branch tips from 4 mice; LT4, $n = 220$ branch tips from 3 mice) (Fig. 3B). In control mice, the maximum branch extension was 79 µm and the maximum branch retraction was 200 µm. Overall, control mice exhibited a net reduction in axonal branch length (–4.52 ± 1.52 µm). In contrast, changes in MMI mice where the maximum branch extension was 120 µm and the maximum branch retraction was 80 µm culminated in an overall increase in axonal branch length, which was significantly different from control mice (4.07 ± 2.31 µm; $P = 0.0019$, 95% CI (–14.18, –3.38), bootstrap test; Fig. 3B). Like control mice, LT4 mice also displayed an overall reduction in axonal branch length; however, the maximum branch extension was 104 µm and the maximum branch retraction was 574 µm, resulting in a significantly greater reduction of branch tip lengths than control mice (–17.08 ± 4.93 µm; $P = 0.014$, 95% CI (3.24, 23.36), bootstrap test; Fig. 3B). The changes of overall axonal branch length between MMI and LT4 mice were also significantly different ($P < 0.001$ 95% CI (11.21, 32.57), bootstrap test).

Axonal branches that exhibited changes in length above the measurement noise threshold (see Materials and Methods) were next sorted into groups of positive- or negative-going changes in length (i.e., extensions or retractions, respectively) and the means of each group were then calculated. As predicted by the net positive-going changes in branch tip lengths observed in the MMI group, axonal branches exhibited a significant increase in the magnitude of branch tip extensions (control—10.83 ± 1.60 µm, 30.65% of all branches; MMI—14.44 ± 3.04 µm, 41.38% of all branches; $P = 0.031$, 95% CI (–18.45, –1.56), bootstrap test; Fig. 3B) with no significant difference in the magnitude of branch tip retractions relative to controls (control—23.01 ± 3.32 µm, 34.48% of all branches; MMI–16.13 ± 2.79 µm, 26.72% of all branches; $P = 0.10$, 95% CI (–1.39, 15.22), bootstrap test; Fig. 3C). Consistent with the negative-going net changes in branch tip lengths in the LT4 group, there was no significant difference in the magnitude of branch tip extensions (13.27 ± 2.23 µm, 25.45% of all branches; $P = 0.37$, 95% CI (–7.99, 2.62), bootstrap test; Fig. 3C), but there was a significant difference in the magnitude of branch tip retractions relative to controls (45.86 ± 10.27 µm, 44.55% of all branches; $P = 0.035$, 95% CI (–45.95, –3.53), bootstrap

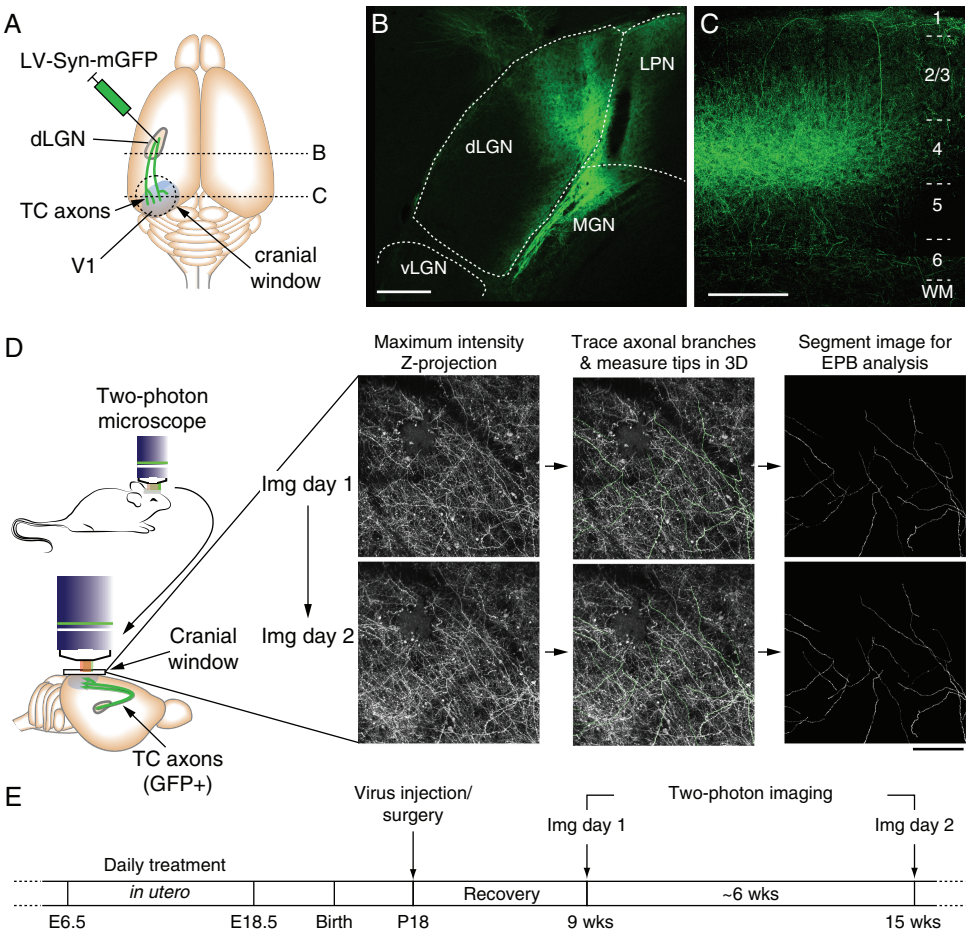

Figure 2. In vivo two-photon imaging of TC axons in V1. (*A*) Cartoon showing the relative locations of LV-Syn-mGFP injections and mGFP-labeled TC axons in V1 and positioning of the cranial window. (*B*) Example confocal images of mGFP labeling in dLGN. Note that GFP signal is largely restricted to the binocular segment of dLGN (i.e., the more medial portion, Coleman et al. 2009). (*C*) Confocal image of TC axons in binocular V1. Note the density of horizontal collateral axonal branches in layer 1, deep layer 2/3 and layer 4 and the lack of GFP-labeled cell bodies, all of which are consistent with TC axon labeling. (*D*) The left panel shows a cartoon of the chronic two-photon imaging preparation and imaging area relative to GFP-labeled TC axons in V1. To the right are shown example two-photon images of the same TC axons in superficial layers of V1 (0–150 μm, bird's eye view) from 2 imaging sessions separated by 54 days. The middle images show an overlay of axonal branch tracings from the image Z-stack on the maximum-intensity projection that were used to measure branch lengths and for segmenting branches for EPB (and axonal backbone) brightness measurements. (*E*) Experimental timeline. (Scale bars = 200 μm).

test; Fig. 3*D*). In addition, while there was no significant difference in the magnitude of branch tip extensions between MMI and LT4 mice, the magnitude of branch tip retractions was significantly greater in LT4 mice compared with MMI mice (extensions: $P = 0.14$, 95% CI (−16.37, 1.76), bootstrap test; retractions: $P = 0.0050$, 95% CI (−51.90, −10.41), bootstrap test).

Although the magnitude of the majority (>60%) of branch tip changes for all groups was <10 μm, the magnitudes and frequencies of larger scale changes in branch tip lengths were greater for the MMI and LT4 groups. To determine whether large-scale changes in axonal branches were more prevalent in MMI and LT4 mice than in control mice, we compared the distribution of branches with length changes greater than the 50th percentile (Fig. 3*E*,*F*). Both MMI and LT4 offspring exhibited significant differences from control offspring in the distribution of branch tip extensions that were well above σ_{noise} ($P < 0.001$, control vs. MMI; $P = 0.005$, control vs. LT4; K–S test, Fig. 4*E*). In addition, large-scale branch tip extensions occurred in MMI mice with significantly greater frequency than they did in LT4 mice ($P = 0.02$; K–S test, Fig. 4*D*). However, there was no significant difference in the distribution of branch retraction lengths between MMI and control mice ($P = 0.25$, K–S test, Fig. 4*E*). Furthermore, there was a significant difference in the distribution of branch retractions in LT4 mice relative to controls, which occurred with greater frequency in LT4 mice ($P = 0.03$, K–S test, Fig. 4*E*). Finally, there was a significant difference in the distributions for the lengths of branch tip retractions between MMI and LT4 mice where the large-scale branch retractions occurred with greater frequency in LT4 mice ($P = 0.04$, MMI vs. LT4; K–S test, Fig. 4*E*).

Overall, these results demonstrate that both prenatal hypo- and hyperthyroidism are associated with a change in the steady-state dynamics of TC axonal branch structure in adult V1. Together, the data suggest that the growth of distal TC axonal branches (and new synapses/connections) occurred on a larger scale in MMI mice relative to controls whereas larger portions of distal TC axonal branches (and synapses/connections) were lost with greater frequency in LT4 mice than in control mice.

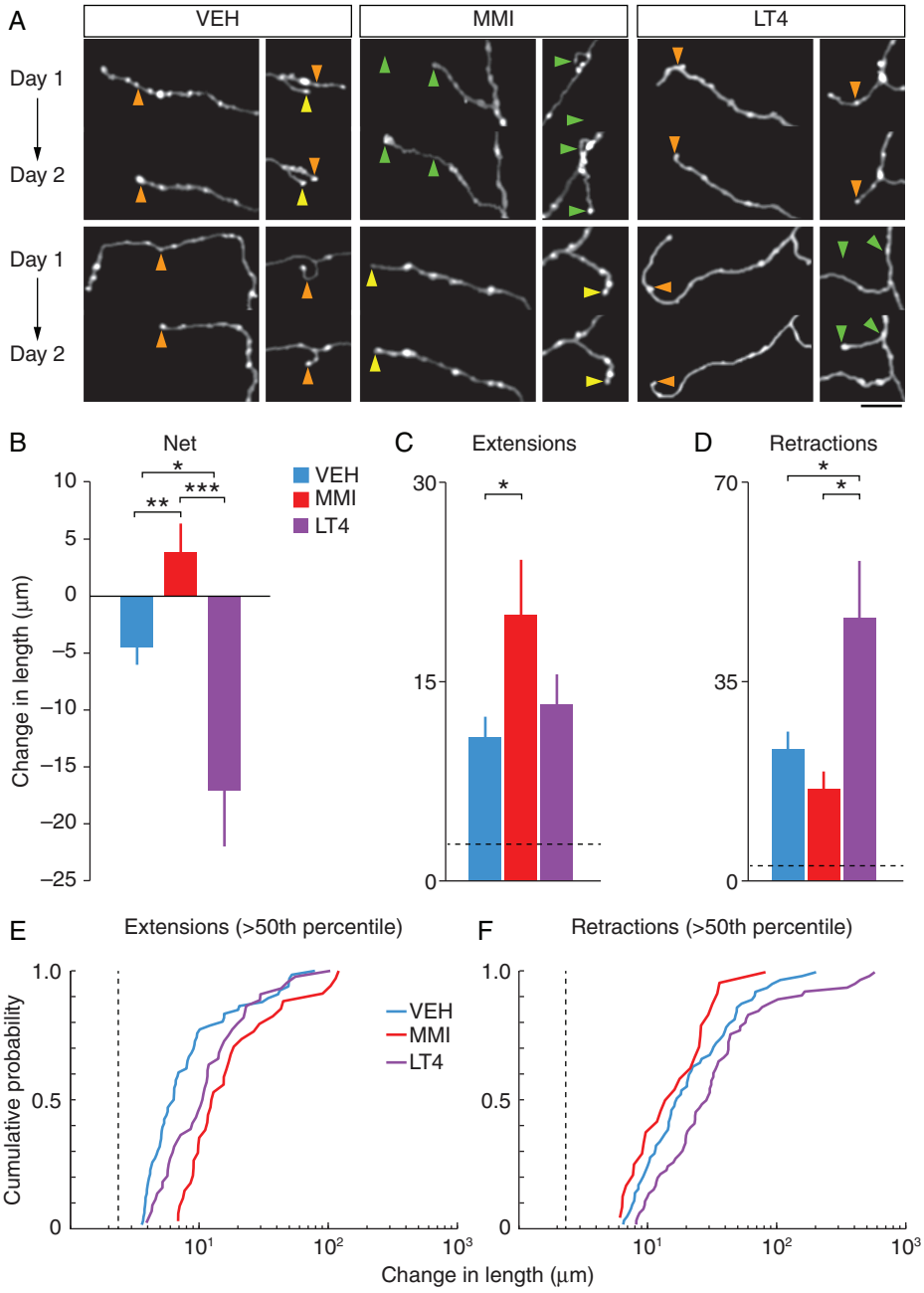

Figure 3. Chronic two-photon imaging reveals atypical structural changes to TC axonal branches in prenatally hypo- (MMI) and hyperthyroid (LT4) mice. (*A*) Two-photon images from each group showing examples of stable (yellow arrowheads), extending (green arrowheads), and retracting (orange arrowheads) branch tips from each group. Each image is a maximum-intensity projection of segmented image *Z*-stacks (see Materials and Methods). (Scale bar = 20 µm) (*B*) Summary of net changes in axonal branch lengths between imaging days 1 and 2. (*C*) The average magnitude of all branch tip extensions (means ± SEM, $^{*}P < 0.05$, $^{**}P < 0.01$, $^{***}P < 0.001$). (*D*) The average magnitude of all branch tip retractions (means ± SEM, $^{*}P < 0.05$). (*E*) Distributions of axonal branch tip extension lengths >50th percentile (means ± SEM, $^{*}P < 0.05$). (*F*) Distributions of axonal branch tip retraction lengths >50th percentile. The dashed lines in *C*–*F* indicate the measurement noise threshold ($2 \times \sigma_{noise}$) used for calculating the means in *C* and *D*.

Prenatal Hypo- and Hyperthyroidism are both Associated with Enhanced EPB Dynamics on TC Axons

To determine whether the differential effects of prenatal hypo- and hyperthyroidism on the stability of distal TC axonal branch tips (and their associated synapses) extend to synapses along more proximal regions of axonal branches, we next characterized the turnover of EPBs along spared portions of these axons in MMI and LT4 mice (Fig. 4A–C). We first compared the percentage of dynamic EPBs (i.e., those lost or gained between imaging sessions) for each group (Fig. 4*D*). The majority (74–92%) of classified boutons for all groups were stable. However, there was a significant difference in the proportion of dynamic EPBs across groups, which was increased in both the MMI and LT4 groups compared with controls (control: 8.3 ± 1.2%; MMI: 24.1 ± 2.7%; LT4: 12.2 ± 1.3%; $P = 0.027$, K–W test; Fig. 4*D*). In addition, the percentage of dynamic EPBs was significantly greater in MMI mice versus LT4 mice ($P < 0.001$, 95% CI (6.95, 16.42), bootstrap test). Among these dynamic

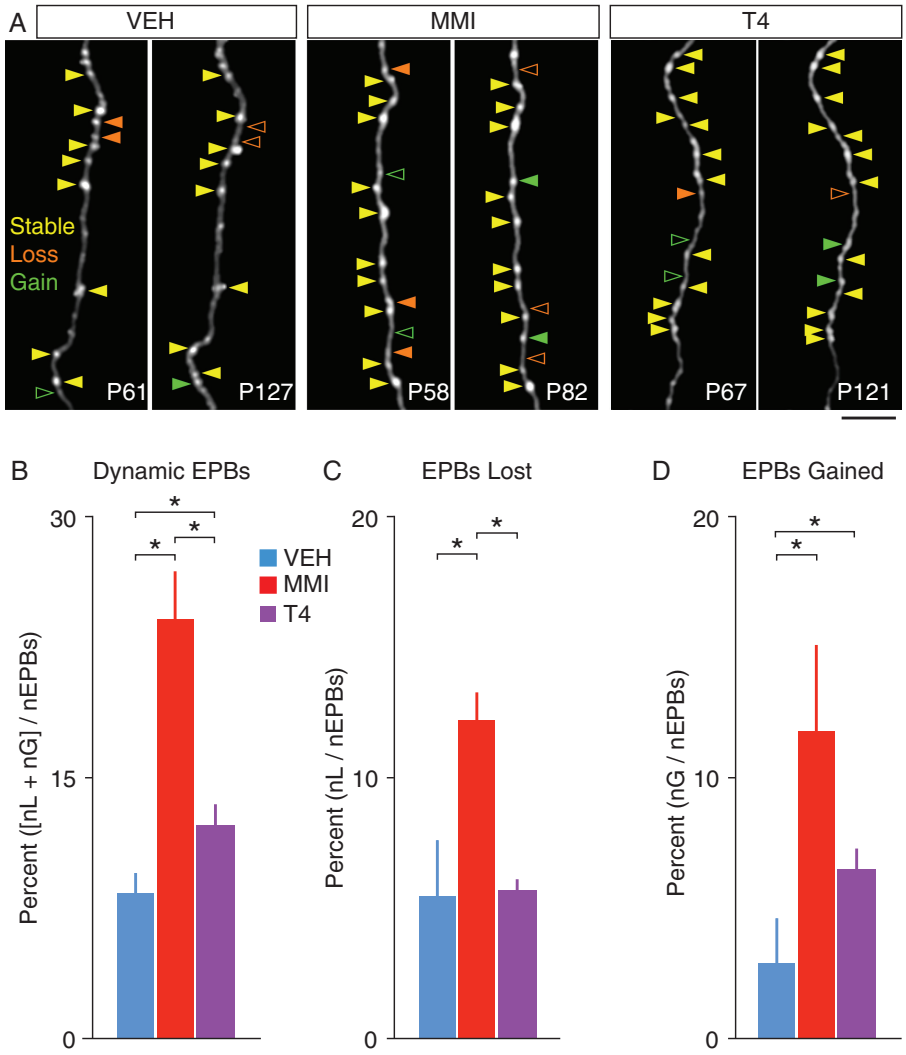

Figure 4. Summary of EPB turnover in TC axons. (*A*) Example two-photon images showing example EPB changes between imaging days from each group (solid arrowhead = EPB present, open arrowhead = EPB absent). (*B*) Summary of overall EPB dynamics (means ± SEM, *$P < 0.05$). (*C*) Summary of EPB losses (means ± SEM, *$P < 0.05$). (*D*) Summary of EPB gains (nL, number lost; nG, number gained; nEPBs, total number of EPBs; means ± SEM, *$P < 0.05$). (Scale bar = 25 μm).

EPBs, there was a significant increase in the percentage lost between imaging sessions in MMI mice compared with control mice (control: 5.5 ± 2.1%, MMI: 12.3 ± 1.0%; $P < 0.001$, 95% CI (–0.10, –0.0027), bootstrap test; Fig. 4*E*). In contrast, the percentage of EPBs lost between imaging sessions in LT4 mice (5.7 ± 0.5%) was not significantly different from control mice ($P = 0.92$, 95% CI (–0.029, 0.040), bootstrap test; Fig. 4*E*). Furthermore, the percentage of lost EPBs was significantly greater in MMI mice than in LT4 mice ($P < 0.001$, 95% CI (0.047, 0.083), bootstrap test). However, both MMI and LT4 mice exhibited a significant increase in the percentage of EPBs gained between imaging sessions relative to control mice (control: 2.9 ± 1.8%; MMI: 11.8 ± 3.3%; LT4: 6.5 ± 0.8%; $P = 0.004$, 95% CI (–0.144, –0.023) control vs. MMI; $P = 0.02$, 95% CI (–0.066, –0.0047) control vs. LT4; bootstrap tests; Fig. 4*F*), but were not significantly different from each other ($P = 0.052$, 95% CI (–0.0095, 0.098), bootstrap test).

Together, these results demonstrate that like distal branch tips, EPBs along more proximal TC axonal regions displayed a change in steady-state dynamics in prenatally hypo- and hyperthyroid adult mice, which was revealed by a decrease in their stability between imaging sessions.

Discussion

To our knowledge, this is the first study to examine and compare the long-term effects of prenatal hypothyroidism and hyperthyroidism on a specific neocortical circuit. While our mouse model of prenatal hypothyroidism was consistent with mild maternal hypothyroidism, we were still able to detect significant effects on the stability of TC axons in these mice. In addition, the fact that we observed significant effects of maternal hyperthyroidism on TC axonal structure in adult offspring supports the idea that excessive maternal T4 does indeed adversely affect fetal levels and/or neural development (Porreco and Bloch 1990; Burrow et al. 1994; Luton et al. 2005; Stagnaro-Green and Pearce 2012). Interestingly, the lower birthrates observed in our mouse model of prenatal hyperthyroidism (Supplementary Table 1) mirrors the increased incidence of miscarriages in women with hyperthyroidism during pregnancy (Stagnaro-Green and Pearce 2012). A major finding of this study is that both hypo- and hyperthyroidism restricted to prenatal development negatively affected steady-state structural dynamics of TC axons in the adult neocortex. In addition, our results suggest

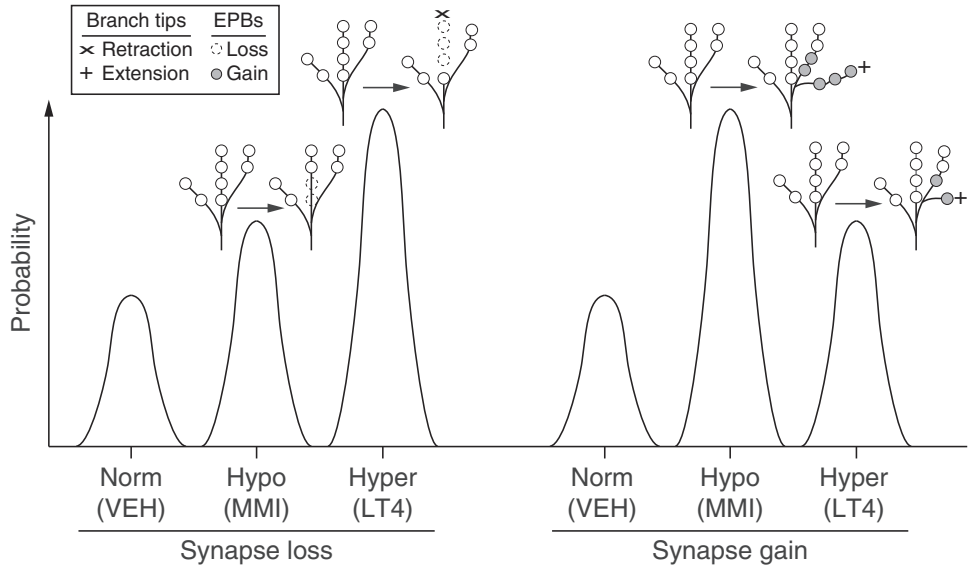

Figure 5. Model summarizing the opposing effects of prenatal hypo- and hyperthyroidism on TC axonal branch and EPB steady-state dynamics in adult V1. The probability of TC synapse losses or gains is schematized for each experimental group. TC synapses are more likely to be lost in mice with prenatal hypo- (Hypo/MMI) or hyperthyroidism (Hyper/LT4) versus control mice (Norm/VEH). However, the prevalence of large-scale branch retractions is greater in mice with prenatal hyperthyroidism as synapse loss was only mediated by smaller-scale changes in EPBs for mice with prenatal hypothyroidism. The probability of TC synapse addition through the growth of distal branches and EPB growth on more proximal regions is increased in both mice with prenatal hypo- and hyperthyroidism. However, the probability of gaining new synapses is greatest in mice with prenatal hypothyroidism due to a significant increase of branch growth over control mice.

that TC synaptic stability is differentially affected between the 2 conditions. Hypothyroid offspring displayed structural changes to TC axons that were indicative of excessive synaptic growth. In contrast, hyperthyroid offspring displayed changes indicative of excessive synaptic loss (Fig. 5). While further studies are required to determine the functional impact of the excessive TC synapse loss we observed in this study, our findings reinforce the notion that hypothyroidism should be carefully managed during pregnancy, and that hyperthyroidism (e.g., Graves' disease) may warrant the same attention (Davidson et al. 1991; Burrow et al. 1994; Bongers-Schokking and de Muinck Keizer-Schrama 2005; Luton et al. 2005; Stagnaro-Green and Pearce 2012).

The majority of cortical connections becomes stable as the brain matures through an increase in synaptic tenacity, which is a feature of cortical circuits essential for preserving learned functions and behavioral adaptations (Minerbi et al. 2009). However, the adult neocortex does maintain a relatively small yet functionally significant fraction of synapses pervious to change (Gogolla et al. 2007; Holtmaat and Svoboda 2009). For example, TC axonal structure and connectivity are sensitive to changes in cortical excitability caused by sensory deprivation (Oberlaender et al. 2012). It is possible that early effects of hypo- and hyperthyroidism cause long-term changes in the excitability of cortical neurons and networks, which in turn disrupts the structural stability of TC circuitry in adulthood. γ-Aminobutyric acid levels were shown to increase and decrease in rat models of perinatal hypo- and hyperthyroidism, respectively (Ahmed et al. 2010). This observation lead the authors to suggest that overall excitability in the adult brain could be decreased by insufficient TH levels and increased by excessive TH levels. However, severe perinatal hypothyroidism in rats causes lasting reductions in the densities of parvalbumin-positive interneuron processes and puncta in neocortex, suggesting that the excitability of cortical neurons may be enhanced (Berbel et al. 1996). In addition, excitability could be further altered by abnormal white matter development. TH directly regulate the expression of key genes involved in oligodendrocyte differentiation and function (Ibarrola and Rodriguez-Pena 1997; Barradas et al. 2001; Dugas et al. 2012). Further, hypothyroidism in rodents (Malone et al. 1975; Walters and Morell 1981) and humans (Gupta et al. 1995; Jagannathan et al. 1998) is accompanied by reductions in white matter, and myelin development is accelerated in hyperthyroid rats (Walters and Morell 1981). In vivo electrophysiological or calcium imaging studies of spontaneous and stimulus-driven neural activity and detailed morphological examination of axons in V1 could help shed light on how cortical activity and/or neuronal excitability is affected by perturbations in prenatal T4 levels.

It is important to consider how changes in TC input on the scale we observed in this study could impact cortical function. Detailed neuroanatomical studies show that TC synapses account for a relatively small fraction (< 15% of synapses out of thousands) of synapses on individual visual cortical neurons (Ahmed et al. 1994). Despite this apparent scarcity of synaptic input, TC synapses exert a strong influence on cortical activity (Bruno and Sakmann 2006; Schoonover et al. 2014). Indeed, even a rather modest decrease in TC synaptic density is sufficient to cause significant functional response depression in mouse V1 that results in behavioral impairment (Iny et al. 2006; Coleman et al. 2010; Khibnik et al. 2010). Moreover, since mouse TC axons contain an estimated 2–3 boutons/10 μm, branch retractions or extensions in the range of 10–20 μm would culminate in significant synaptic turnover (Tettoni et al. 1998). When further combined with the increases in EPB dynamics that were observed in hypo- and hyperthyroid offspring, it is likely that hundreds of synaptic connections per axon were affected. Thus, the increased structural changes observed for hypo- and hyperthyroid offspring would be expected to have a significant functional impact in V1, even if these changes were limited to a subset of axonal branches (e.g., 25%–50% of an estimated 200 branches/axon). However, more detailed anatomical studies are required to determine the extent to which synapses are affected in other

cortical layers, especially layer 4 where TC synapses are most concentrated.

Together, our findings raise the possibility that sensory processing and learning deficits associated with prenatal hypo- and hyperthyroidism result from more than just static defects in cortical architecture, but also from accumulating and persistent defects in synaptic stability and steady-state dynamics in cortical circuits (Minerbi et al. 2009; Fisher-Lavie et al. 2011; Berbel et al. 2014; Deisseroth 2014; Gunaydin et al. 2014). There is some indication from the data presented here that steady-state dynamics of TC synapses may be altered in an attempt to compensate for synaptic loss through the addition of new synapses, which appears to occur on a larger scale in hypothyroid offspring (Fig. 5). While such apparent compensation could serve to ameliorate functional deficits, it is equally likely to underlie maladaptive changes in the circuitry that could exacerbate deficits in neural function and/or plasticity (Deisseroth 2014). The latter scenario is consistent with clinical findings that pre- and postnatal hypothyroidism is associated with persistent deficits in contrast sensitivity, visual processing, and visuomotor and visuospatial abilities in humans (Mirabella et al. 2000, 2005; Zoeller and Rovet 2004; Simic et al. 2013).

TC input to layer 1 of V1 presumably targets the spines of apical dendritic tufts of pyramidal neurons from most or all cortical layers (Petreanu et al. 2009; Rubio-Garrido et al. 2009; Cruikshank et al. 2012). In addition to relaying core visual information, these inputs are thought to be crucial for feedback interactions in cerebral cortex that underlie cognitive processes such as associative learning and attention (Sjostrom and Hausser 2006; Gilbert and Sigman 2007; Cruz-Martin et al. 2014). Thus, it is possible that a steady net loss of layer 1 TC synapses over the lifetime of hypo- and hyperthyroid offspring progressively degrades feedback required for proper processing of visual information relayed to "higher" cortical areas. It is also possible that overall activation of V1 is weakened by reduced synaptic drive from TC input, which in itself could serve to increase synaptic turnover (Bastrikova et al. 2008; Becker et al. 2008; Hofer et al. 2009; Coleman et al. 2010; Wiegert and Oertner 2013).

In conclusion, our in vivo observations suggest that prenatal hypo- and hyperthyroidism can cause persistent, maladaptive changes to circuitry involved in the early stages of sensory processing and plasticity in the neocortex. Further, the models developed here lay the groundwork for future studies that can take full advantage of the transgenic capabilities in mice (e.g., using cell-specific Cre lines to selectively label subpopulations of neurons for imaging). Interestingly, our findings support the concept of fetal programming by early hypo- and hyperthyroidism (Andersen et al. 2015), which may serve to prime the brain for psychiatric disease including schizophrenia (Santos et al. 2012; Gyllenberg et al. 2015) and autism spectrum disorder (Berbel et al. 2014; Andersen et al. 2015). It is noteworthy that results from a recent genome-wide association study point to excessive synaptic pruning as a key neurobiological mechanism of schizophrenia (Sekar et al. 2016). Additional studies are warranted to link atypical changes in synaptic connectivity in hypo- and hyperthyroid offspring to functional deficits as well as learning, behavior and disease, studies for which the mouse visual system is well suited (Keller et al. 2012; Gavornik and Bear 2014; Cooke et al. 2015).

Supplementary Material

Supplementary material can be found at: http://www.cercor.oxfordjournals.org/.

Funding

This work was supported by the National Institutes of Health (HD065200 to S.A.R.) and the Children's Miracle Network (J.E.C.).

Notes

We thank Dr Matthew Sarkisian for helpful discussions and comments. We also acknowledge and thank the anonymous referees for invaluable comments and suggestions. We thank Giselle Gomez, Arjith Rathakrishnan, and Dr Hangning Zhang for excellent administrative and technical support. *Conflict of Interest*: None declared.

References

Ahmed B, Anderson JC, Douglas RJ, Martin KA, Nelson JC. 1994. Polyneuronal innervation of spiny stellate neurons in cat visual cortex. J Comp Neurol. 341:39–49.

Ahmed OM, Abd El-Tawab SM, Ahmed RG. 2010. Effects of experimentally induced maternal hypothyroidism and hyperthyroidism on the development of rat offspring: I. The development of the thyroid hormones-neurotransmitters and adenosinergic system interactions. Int J Dev Neurosci. 28:437–454.

Ahmed OM, Ahmed RG, El-Gareib AW, El-Bakry AM, Abd El-Tawab SM. 2012. Effects of experimentally induced maternal hypothyroidism and hyperthyroidism on the development of rat offspring: II-the developmental pattern of neurons in relation to oxidative stress and antioxidant defense system. Int J Dev Neurosci. 30:517–537.

Altman DG, Bland JM. 2011. How to obtain the P value from a confidence interval. BMJ. 343:d2304.

Andersen SL, Olsen J, Laurberg P. 2015. Foetal programming by maternal thyroid disease. Clin Endocrinol. 83:751–758.

Antonini A, Stryker MP. 1993. Rapid remodeling of axonal arbors in the visual cortex. Science. 260:1819–1821.

Auso E, Cases O, Fouquet C, Camacho M, Garcia-Velasco JV, Gaspar P, Berbel P. 2001. Protracted expression of serotonin transporter and altered thalamocortical projections in the barrelfield of hypothyroid rats. Eur J Neurosci. 14:1968–1980.

Barradas PC, Vieira RS, De Freitas MS. 2001. Selective effect of hypothyroidism on expression of myelin markers during development. J Neurosci Res. 66:254–261.

Bastrikova N, Gardner GA, Reece JM, Jeromin A, Dudek SM. 2008. Synapse elimination accompanies functional plasticity in hippocampal neurons. Proc Natl Acad Sci USA. 105:3123–3127.

Becker N, Wierenga CJ, Fonseca R, Bonhoeffer T, Nagerl UV. 2008. LTD induction causes morphological changes of presynaptic boutons and reduces their contacts with spines. Neuron. 60:590–597.

Berbel P, Guadano-Ferraz A, Martinez M, Quiles JA, Balboa R, Innocenti GM. 1993. Organization of auditory callosal connections in hypothyroid adult rats. Eur J Neurosci. 5:1465–1478.

Berbel P, Marco P, Cerezo JR, DeFelipe J. 1996. Distribution of parvalbumin immunoreactivity in the neocortex of hypothyroid adult rats. Neurosci Lett. 204:65–68.

Berbel P, Navarro D, Auso E, Varea E, Rodriguez AE, Ballesta JJ, Salinas M, Flores E, Faura CC, de Escobar GM. 2010. Role of late maternal thyroid hormones in cerebral cortex development: an experimental model for human prematurity. Cereb Cortex. 20:1462–1475.

Berbel P, Navarro D, Roman GC. 2014. An evo-devo approach to thyroid hormones in cerebral and cerebellar cortical

development: etiological implications for autism. Front Endocrinol. 5:146.

Berbel PJ, Escobar del Rey F, Morreale de Escobar G, Ruiz-Marcos A. 1985. Effect of hypothyroidism on the size of spines of pyramidal neurons of the cerebral cortex. Brain Res. 337:217–223.

Bongers-Schokking JJ, de Muinck Keizer-Schrama SM. 2005. Influence of timing and dose of thyroid hormone replacement on mental, psychomotor, and behavioral development in children with congenital hypothyroidism. J Pediatr. 147: 768–774.

Bruno AN, Da Silva RS, Bonan CD, Battastini AM, Barreto-chaves ML, Sarkis JJ. 2003. Hyperthyroidism modifies ectonucleotidase activities in synaptosomes from hippocampus and cerebral cortex of rats in different phases of development. Int J Dev Neurosci. 21:401–408.

Bruno RM, Sakmann B. 2006. Cortex is driven by weak but synchronously active thalamocortical synapses. Science. 312:1622–1627.

Burrow GN, Fisher DA, Larsen PR. 1994. Maternal and fetal thyroid function. N Engl J Med. 331:1072–1078.

Calvo R, Obregon MJ, Ruiz de Ona C, Escobar del Rey F, Morreale de Escobar G. 1990. Congenital hypothyroidism, as studied in rats. Crucial role of maternal thyroxine but not of 3,5,3′-triiodothyronine in the protection of the fetal brain. J Clin Invest. 86:889–899.

Calvo RM, Jauniaux E, Gulbis B, Asuncion M, Gervy C, Contempre B, Morreale de Escobar G. 2002. Fetal tissues are exposed to biologically relevant free thyroxine concentrations during early phases of development. J Clin Endocrinol Metab. 87:1768–1777.

Canty AJ, Huang L, Jackson JS, Little GE, Knott G, Maco B, De Paola V. 2013. In-vivo single neuron axotomy triggers axon regeneration to restore synaptic density in specific cortical circuits. Nat Commun. 4:2038.

Coleman JE, Law K, Bear MF. 2009. Anatomical origins of ocular dominance in mouse primary visual cortex. Neuroscience. 161:561–571.

Coleman JE, Nahmani M, Gavornik JP, Haslinger R, Heynen AJ, Erisir A, Bear MF. 2010. Rapid structural remodeling of thalamocortical synapses parallels experience-dependent functional plasticity in mouse primary visual cortex. J Neurosci. 30:9670–9682.

Cooke SF, Komorowski RW, Kaplan ES, Gavornik JP, Bear MF. 2015. Visual recognition memory, manifested as long-term habituation, requires synaptic plasticity in V1. Nat Neurosci. 18:262–271.

Cooper DS, Kieffer JD, Saxe V, Mover H, Maloof F, Ridgway EC. 1984. Methimazole pharmacology in the rat: studies using a newly developed radioimmunoassay for methimazole. Endocrinology. 114:786–793.

Cruikshank SJ, Ahmed OJ, Stevens TR, Patrick SL, Gonzalez AN, Elmaleh M, Connors BW. 2012. Thalamic control of layer 1 circuits in prefrontal cortex. J Neurosci. 32:17813–17823.

Cruz-Martin A, El-Danaf RN, Osakada F, Sriram B, Dhande OS, Nguyen PL, Callaway EM, Ghosh A, Huberman AD. 2014. A dedicated circuit links direction-selective retinal ganglion cells to the primary visual cortex. Nature. 507:358–361.

Daneman D, Howard NJ. 1980. Neonatal thyrotoxicosis: intellectual impairment and craniosynostosis in later years. J Pediatr. 97:257–259.

Davidson KM, Richards DS, Schatz DA, Fisher DA. 1991. Successful in utero treatment of fetal goiter and hypothyroidism. N Engl J Med. 324:543–546.

Deisseroth K. 2014. Circuit dynamics of adaptive and maladaptive behaviour. Nature. 505:309–317.

Delahunty C, Falconer S, Hume R, Jackson L, Midgley P, Mirfield M, Ogston S, Perra O, Simpson J, Watson J, et al. 2010. Levels of neonatal thyroid hormone in preterm infants and neurodevelopmental outcome at 5 1/2 years: millennium cohort study. J Clin Endocrinol Metab. 95:4898–4908.

De Paola V, Holtmaat A, Knott G, Song S, Wilbrecht L, Caroni P, Svoboda K. 2006. Cell type-specific structural plasticity of axonal branches and boutons in the adult neocortex. Neuron. 49:861–875.

Dittgen T, Nimmerjahn A, Komai S, Licznerski P, Waters J, Margrie TW, Helmchen F, Denk W, Brecht M, Osten P. 2004. Lentivirus-based genetic manipulations of cortical neurons and their optical and electrophysiological monitoring in vivo. Proc Natl Acad Sci USA. 101:18206–18211.

Dugas JC, Ibrahim A, Barres BA. 2012. The T3-induced gene KLF9 regulates oligodendrocyte differentiation and myelin regeneration. Mol Cell Neurosci. 50:45–57.

Fisher-Lavie A, Zeidan A, Stern M, Garner CC, Ziv NE. 2011. Use dependence of presynaptic tenacity. J Neurosci. 31:16770–16780.

Gavornik JP, Bear MF. 2014. Higher brain functions served by the lowly rodent primary visual cortex. Learn Mem. 21:527–533.

Gilbert CD, Sigman M. 2007. Brain states: top-down influences in sensory processing. Neuron. 54:677–696.

Gilbert ME, Lasley SM. 2013. Developmental thyroid hormone insufficiency and brain development: a role for brain-derived neurotrophic factor (BDNF)? Neuroscience. 239:253–270.

Gilbert ME, Ramos RL, McCloskey DP, Goodman JH. 2014. Subcortical band heterotopia in rat offspring following maternal hypothyroxinaemia: structural and functional characteristics. J Neuroendocrinol. 26:528–541.

Gilbert ME, Sui L, Walker MJ, Anderson W, Thomas S, Smoller SN, Schon JP, Phani S, Goodman JH. 2007. Thyroid hormone insufficiency during brain development reduces parvalbumin immunoreactivity and inhibitory function in the hippocampus. Endocrinology. 148:92–102.

Gogolla N, Galimberti I, Caroni P. 2007. Structural plasticity of axon terminals in the adult. Curr Opin Neurobiol. 17:516–524.

Gravel C, Hawkes R. 1990. Maturation of the corpus callosum of the rat: I. Influence of thyroid hormones on the topography of callosal projections. J Comp Neurol. 291:128–146.

Gravel C, Sasseville R, Hawkes R. 1990. Maturation of the corpus callosum of the rat: II. Influence of thyroid hormones on the number and maturation of axons. J Comp Neurol. 291:147–161.

Grillo FW, Song S, Teles-Grilo Ruivo LM, Huang L, Gao G, Knott GW, Maco B, Ferretti V, Thompson D, Little GE, et al. 2013. Increased axonal bouton dynamics in the aging mouse cortex. Proc Natl Acad Sci USA. 110:E1514–E1523.

Gunaydin LA, Grosenick L, Finkelstein JC, Kauvar IV, Fenno LE, Adhikari A, Lammel S, Mirzabekov JJ, Airan RD, Zalocusky KA, et al. 2014. Natural neural projection dynamics underlying social behavior. Cell. 157:1535–1551.

Gupta RK, Bhatia V, Poptani H, Gujral RB. 1995. Brain metabolite changes on in vivo proton magnetic resonance spectroscopy in children with congenital hypothyroidism. J Pediatr. 126: 389–392.

Gyllenberg D, Sourander A, Surcel HM, Hinkka-Yli-Salomaki S, McKeague IW, Brown AS. 2015. Hypothyroxinemia during gestation and offspring Schizophrenia in a National Birth Cohort. Biol Psychiatry. doi:10.1016/j.biopsych.2015.06.014.

Hofer SB, Mrsic-Flogel TD, Bonhoeffer T, Hubener M. 2009. Experience leaves a lasting structural trace in cortical circuits. Nature. 457:313–317.

Holtmaat A, Svoboda K. 2009. Experience-dependent structural synaptic plasticity in the mammalian brain. Nat Rev Neurosci. 10:647–658.

Horn S, Heuer H. 2010. Thyroid hormone action during brain development: more questions than answers. Mol Cell Endocrinol. 315:19–26.

Ibarrola N, Rodriguez-Pena A. 1997. Hypothyroidism coordinately and transiently affects myelin protein gene expression in most rat brain regions during postnatal development. Brain Res. 752:285–293.

Iny K, Heynen AJ, Sklar E, Bear MF. 2006. Bidirectional modifications of visual acuity induced by monocular deprivation in juvenile and adult rats. J Neurosci. 26:7368–7374.

Ipina SL, Ruiz-Marcos A, Escobar del Rey F, Morreale de Escobar G. 1987. Pyramidal cortical cell morphology studied by multivariate analysis: effects of neonatal thyroidectomy, ageing and thyroxine-substitution therapy. Brain Res. 465:219–229.

Jagannathan NR, Tandon N, Raghunathan P, Kochupillai N. 1998. Reversal of abnormalities of myelination by thyroxine therapy in congenital hypothyroidism: localized in vivo proton magnetic resonance spectroscopy (MRS) study. Brain Res Dev Brain Res. 109:179–186.

Keller GB, Bonhoeffer T, Hubener M. 2012. Sensorimotor mismatch signals in primary visual cortex of the behaving mouse. Neuron. 74:809–815.

Khibnik LA, Cho KK, Bear MF. 2010. Relative contribution of feedforward excitatory connections to expression of ocular dominance plasticity in layer 4 of visual cortex. Neuron. 66:493–500.

Koibuchi N, Chin WW. 2000. Thyroid hormone action and brain development. Trends Endocrinol Metab. 11:123–128.

Kopelman AE. 1983. Delayed cerebral development in twins with congenital hyperthyroidism. Am J Dis Children. 137:842–845.

Lasley SM, Gilbert ME. 2011. Developmental thyroid hormone insufficiency reduces expression of brain-derived neurotrophic factor (BDNF) in adults but not in neonates. Neurotoxicol Teratol. 33:464–472.

Lauder JM. 1977. The effects of early hypo- and hyperthyroidism on the development of rat cerebellar cortex. III. Kinetics of cell proliferation in the external granular layer. Brain Res. 126:31–51.

Lauder JM. 1978. Effects of early hypo- and hyperthyroidism on development of rat cerebellar cortex. IV. The parallel fibers. Brain Res. 142:25–39.

Lucio RA, Garcia JV, Ramon Cerezo J, Pacheco P, Innocenti GM, Berbel P. 1997. The development of auditory callosal connections in normal and hypothyroid rats. Cereb Cortex. 7:303–316.

Luton D, Le Gac I, Vuillard E, Castanet M, Guibourdenche J, Noel M, Toubert ME, Leger J, Boissinot C, Schlageter MH, et al. 2005. Management of Graves' disease during pregnancy: the key role of fetal thyroid gland monitoring. J Clin Endocrinol Metab. 90:6093–6098.

Mallela MK, Strobl M, Poulsen RR, Wendler CC, Booth CJ, Rivkees SA. 2014. Evaluation of developmental toxicity of propylthiouracil and methimazole. Dev Reprod Toxicol. 101:300–307.

Malone MJ, Rosman NP, Szoke M, Davis D. 1975. Myelination of brain in experimental hypothyroidism. An electron-microscopic and biochemical study of purified myelin isolates. J Neurol Sci. 26:1–11.

Marta CB, Adamo AM, Soto EF, Pasquini JM. 1998. Sustained neonatal hyperthyroidism in the rat affects myelination in the central nervous system. J Neurosci Res. 53:251–259.

Minerbi A, Kahana R, Goldfeld L, Kaufman M, Marom S, Ziv NE. 2009. Long-term relationships between synaptic tenacity, synaptic remodeling, and network activity. PLoS Biol. 7: e1000136.

Mirabella G, Feig D, Astzalos E, Perlman K, Rovet JF. 2000. The effect of abnormal intrauterine thyroid hormone economies on infant cognitive abilities. J Pediatr Endocrinol Metab. 13:191–194.

Mirabella G, Westall CA, Asztalos E, Perlman K, Koren G, Rovet J. 2005. Development of contrast sensitivity in infants with prenatal and neonatal thyroid hormone insufficiencies. Pediatr Res. 57:902–907.

Mostany R, Portera-Cailliau C. 2008. A craniotomy surgery procedure for chronic brain imaging. J Vis Exp. 12:e680. doi:10.3791/680.

Navarro D, Alvarado M, Morte B, Berbel D, Sesma J, Pacheco P, Morreale de Escobar G, Bernal J, Berbel P. 2014. Late maternal hypothyroidism alters the expression of Camk4 in neocortical subplate neurons: a comparison with Nurr1 labeling. Cereb Cortex. 24:2694–2706.

Nicholson JL, Altman J. 1972. Synaptogenesis in the rat cerebellum: effects of early hypo- and hyperthyroidism. Science. 176:530–532.

Oberlaender M, Ramirez A, Bruno RM. 2012. Sensory experience restructures thalamocortical axons during adulthood. Neuron. 74:648–655.

Petreanu L, Mao T, Sternson SM, Svoboda K. 2009. The subcellular organization of neocortical excitatory connections. Nature. 457:1142–1145.

Plioplys AV, Gravel C, Hawkes R. 1986. Selective suppression of neurofilament antigen expression in the hypothyroid rat cerebral cortex. J Neurol Sci. 75:53–68.

Porreco RP, Bloch CA. 1990. Fetal blood sampling in the management of intrauterine thyrotoxicosis. Obstet Gynecol. 76:509–512.

Rovet J, Simic N. 2008. The role of transient hypothyroxinemia of prematurity in development of visual abilities. Semin Perinatol. 32:431–437.

Rovet JF. 2014. The role of thyroid hormones for brain development and cognitive function. Endocr Dev. 26:26–43.

Rubio-Garrido P, Perez-de-Manzo F, Porrero C, Galazo MJ, Clasca F. 2009. Thalamic input to distal apical dendrites in neocortical layer 1 is massive and highly convergent. Cereb Cortex. 19:2380–2395.

Ruiz-Marcos A, Cartagena-Abella P, Martinez-Galan JR, Calvo R, Morreale de Escobar G, Escobar del Rey F. 1994. Thyroxine treatment and the recovery of pyramidal cells of the cerebral cortex from changes induced by juvenile-onset hypothyroidism. J Neurobiol. 25:808–818.

Ruiz-Marcos A, Salas J, Sanchez-Toscano F, Escobar del Rey F, Morreale de Escobar G. 1983. Effect of neonatal and adult-onset hypothyroidism on pyramidal cells of the rat auditory cortex. Brain Res. 285:205–213.

Ruiz-Marcos A, Sanchez-Toscano F, Escobar del Rey F, Morreale de Escobar G. 1979. Severe hypothyroidism and the maturation of the rat cerebral cortex. Brain Res. 162:315–329.

Santos NC, Costa P, Ruano D, Macedo A, Soares MJ, Valente J, Pereira AT, Azevedo MH, Palha JA. 2012. Revisiting thyroid hormones in schizophrenia. J Thyroid Res. 2012:569147.

Schoonover CE, Tapia JC, Schilling VC, Wimmer V, Blazeski R, Zhang W, Mason CA, Bruno RM. 2014. Comparative strength and dendritic organization of thalamocortical and corticocortical synapses onto excitatory layer 4 neurons. J Neurosci. 34:6746–6758.

Sekar A, Bialas AR, de Rivera H, Davis A, Hammond TR, Kamitaki N, Tooley K, Presumey J, Baum M, Van Doren V, et al. 2016. Schizophrenia risk from complex variation of complement component 4. Nature. 530:177–183.

Simic N, Khan S, Rovet J. 2013. Visuospatial, visuoperceptual, and visuoconstructive abilities in congenital hypothyroidism. J Int Neuropsychol Soc. 19:1119–1127.

Sjostrom PJ, Hausser M. 2006. A cooperative switch determines the sign of synaptic plasticity in distal dendrites of neocortical pyramidal neurons. Neuron. 51:227–238.

Stagnaro-Green A, Pearce E. 2012. Thyroid disorders in pregnancy. Nat Rev Endocrinol. 8:650–658.

Tettoni L, Gheorghita-Baechler F, Bressoud R, Welker E, Innocenti GM. 1998. Constant and variable aspects of axonal phenotype in cerebral cortex. Cereb Cortex. 8:543–552.

Walters SN, Morell P. 1981. Effects of altered thyroid states on myelinogenesis. J Neurochem. 36:1792–1801.

Wiegert JS, Oertner TG. 2013. Long-term depression triggers the selective elimination of weakly integrated synapses. Proc Natl Acad Sci USA. 110:E4510–E4519.

Wiesel TN. 1999. Early explorations of the development and plasticity of the visual cortex: A personal view. J Neurobiol. 41:7–9.

Williams F, Watson J, Ogston S, Hume R, Willatts P, Visser T, Scottish Preterm Thyroid G. 2012. Mild maternal thyroid dysfunction at delivery of infants born </=34 weeks and neurodevelopmental outcome at 5.5 years. J Clin Endocrinol Metab. 97:1977–1985.

Zoeller RT, Rovet J. 2004. Timing of thyroid hormone action in the developing brain: clinical observations and experimental findings. J Neuroendocrinol. 16:809–818.